JOURNAL OF THEORETICAL AND APPLIED MECHANICS
55, 1, pp. 265-280, Warsaw 2017
DOI: 10.15632/jtam-pl.55.1.265

DESIGN AND IMPLEMENTATION OF IMPROVED SLIDING MODE CONTROLLER ON 6R MANIPULATOR

Moharam H. Korayem, Saeed R. Nekoo, Alireza Khademi, Faezeh Abdollahi
Robotic Research Laboratory, Center of Excellence in Experimental Solid Mechanics and Dynamics, School of Mechanical Engineering, Iran University of Science and Technology (IUST), Tehran, Iran
e-mail: saerafee@yahoo.com

In this work, we present an improved sliding mode control (ISMC) technique designed and implemented for control of 6R manipulator. Sliding mode control (SMC) is a well-known nonlinear robust method for controlling systems in the presence of uncertainties and disturbances and systems with complex dynamics as in manipulators. Despite this good property, it is difficult to implement this method for the manipulator with a complex structure and more than three degree-of-freedom because of the complicated and massive equation and chattering phenomenon as a property of SMC in control inputs. Here, the chattering phenomenon is eliminated by using an effective algorithm called ISMC and implemented to 6R manipulator by using a low-cost control board based on an ARM microcontroller with high accuracy and memory. The carrying load is considered as the uncertainty for the manipulator, while the dynamic load carrying capacity (DLCC) is considered as a robot performance criterion showing robustness of the controller. The results of simulations and experiments show that the proposed approach has a good performance and is suitable and practical to be applied for manipulators.

Keywords: improved sliding mode control, chattering, DLCC, hardware implementation

1. Introduction

Models of manipulators are complex nonlinear dynamical systems with uncertainties due to differences between mathematical models and real robots. The sliding mode control (SMC) is one of the methods in the category of nonlinear control capable of controlling systems with uncertainties. The SMC technique and the improved SMC (ISMC)-based algorithms have been used frequently in the field of manipulator control. One of the benefits of the SMC is insensitivity to variation of parameters such as load for manipulating. Since the dynamics of manipulators is so complicated, the ISMC method is selected for controlling the system in this work. And yet a lot of work in this field has been applied. Ertugrul *et al.* (2000) presented gain adaptation in SMC of robotic manipulators via MIT rule. The method was implemented on a two-link planar manipulator to validate the proposed algorithm. Vega *et al.* (2003) presented dynamic sliding PID control for trajectory tracking on manipulators. Implementation and comparative experimental study on a two-DOF robot arm were expressed via PD, PID, adaptive and SMC method. Shi *et al.* (2008) expressed robust control of robotic manipulators based on the integral sliding mode. Capisani and Ferrara (2009) used a second-order SMC approach and presented experimental test on COMAU SMART3-S2 rigid industrial manipulator with three joints. Korayem *et al.* (2009) presented the observer-based SMC for determining the dynamic load-carrying capacity of manipulators. Islam and Liu (2011) applied the SMC method for overcoming the problem of large-scale uncertainties in control of manipulators. The parameter uncertainties and external disturbances were considered in the modelling. Foster and Harrison (2011) expressed the experimental investigation of a 5-DOF robot arm with SMC. The method was simulated and verified

with the experimental results. Islam *et al.* (2014) applied SMC and CTC control methods for a multi-DOF articulated robotic arm manipulator and demonstrated superior performance of the SMC by simulation results of a 6-DOF robot manipulator.

The chattering phenomenon is one of the SMC difficulties. This phenomenon occurs because of the existence of switching nature in the sliding mode controller. It is unwanted and leads to an excessive usage of actuator; therefore, the control law may become impractical. Many methods have been proposed for eliminating or reducing the chattering including the boundary layer, continuous approximations and higher order SMC methods. The methods also include synthesized SMC with other techniques such as the fuzzy SMC, adaptive neural network, and optimal SMC (Thangavelusamy and Ponnusamy, 2012; Beyhan *et al.*, 2011; Sefriti *et al.*, 2012; Korayem *et al.*, 2014). Obviation of the chattering phenomenon, in this paper, is the use of ISMC applied to this problem (Ataei *et al.*, 2014).

The model in this paper is a 6R manipulator. The first three links are made as the base of the robot and developed by adding a wrist with three-DOF on that (Jamali *et al.*, 2005; Hamraz *et al.*, 2005). The control system of this manipulator is a digital board with six PIC chips for motors to perform open-loop control. Implementing nonlinear controllers, which are ideal for this manipulator, is not possible. To extend the performance and options of the arm, a new digital board based on ARM LPC1768 CortexM3 microcontroller has been designed and built (Korayem *et al.*, 2013). In the following, we first describe the mathematical model of the manipulator and then design a SMC for it. Then, we briefly describe the control board and, finally, this method is simulated and implemented for the robot.

2. SMC design

SMC is a nonlinear robust control method that is often used in cases that have uncertainty in dynamics and external disturbance. We used this method for its inherent property in robustness and compared to other nonlinear methods. SMC and ISMC are easily implemented.

2.1. SISO system

In order to start the procedure of designing the controller, the dynamical equation should be expressed in the standard form as

$$x^{(n)}(t) = f(\mathbf{x}(t)) + b(\mathbf{x}(t))u(t) \tag{2.1}$$

where the scalar $x(t)$ is the output, the scalar $u(t)$ is the control input and $\mathbf{x}(t) = [x(t), \dot{x}(t), \ldots, x^{(n-1)}(t)]^{\mathrm{T}}$ is the state vector. $f(\mathbf{x}(t))$ is an uncertain nonlinear function bounded by a known continuous function of $\mathbf{x}(t)$, and $b(\mathbf{x}(t))$, similarly, is an uncertain nonlinear function that is of known sign and is bounded by the known continuous function of $\mathbf{x}(t)$.

Consider the uncertainty of parameters in the system, which is denoted as follows

$$f(\mathbf{x}(t)) = (1 + \Delta)\widehat{f}(\mathbf{x}(t)) \qquad b(\mathbf{x}(t)) = (1 + \Delta)\widehat{b}(\mathbf{x}(t)) \tag{2.2}$$

Let the subscript $\widehat{(\cdot)}$ means the system nominal value and symbol Δ means the system uncertainty (small value). The time-varying surface named sliding surface is defined as follows (Slotine and Li, 1991)

$$s(\mathbf{x}(t)) = \Big(\frac{d}{dt} + \lambda\Big)^{n-1}\widetilde{x}(t) \tag{2.3}$$

where λ is a strictly positive constant and $\widetilde{x}(t) = x(t) - x_d(t)$ is the tracking error in the variable $x(t)$. For the second-order system, by considering $n = 2$, the sliding surface is obtained as follows

$$s(\mathbf{x}(t)) = \dot{\tilde{x}}(t) + \lambda\tilde{x}(t) \tag{2.4}$$

The control input law in the sliding mode method is considered as

$$u(t) = u_{eq}(t) + u_{corr}(t) \tag{2.5}$$

where $u_{eq}(t)$ is the equivalent control input and $u_{corr}(t)$ is the correction or switching control input for reaching to the sliding surface when distanced from the sliding surface by the effect of uncertainty and disturbance. $u_{eq}(t)$ is defined by solving $\dot{s}(\mathbf{x}(t)) = 0$ and, therefore, we get

$$u_{eq}(t) = \widehat{b}^{-1}(\mathbf{x}(t))[-\widehat{f}(\mathbf{x}(t)) + \ddot{x}_{desired}(t) - \lambda\dot{\tilde{x}}(t)] \tag{2.6}$$

Hence, $u_{corr}(t)$ is defined as

$$u_{corr}(t) = -\widehat{b}^{-1}(\mathbf{x}(t))k(\mathbf{x}(t))\,\mathrm{sgn}\,(s(\mathbf{x}(t)) \tag{2.7}$$

To reach the sliding surface in finite time, the sliding condition that is defined as follows shall be satisfied

$$\frac{1}{2}s(\mathbf{x}(t))\dot{s}(\mathbf{x}(t)) \leqslant -\eta|s(\mathbf{x}(t))| \tag{2.8}$$

and $\eta > 0$ must be satisfied as well. By assuming

$$\left|\widehat{f}(\mathbf{x}(t)) - f(\mathbf{x}(t))\right| \leqslant f_b \qquad \widehat{b}(\mathbf{x}(t)) = \sqrt{b_{max}b_{min}} \tag{2.9}$$

where f_b is the maximum estimation error in the bound of uncertainty of $f(\mathbf{x}(t))$, b_{max} and b_{min} are the maximum and minimum estimation errors, respectively, in the bound of $b(\mathbf{x}(t))$ and considering (Slotine and Li, 1991)

$$k(\mathbf{x}(t)) \geqslant \beta(f_b + \eta) + (\beta - 1)|u_{eq}(t)| \tag{2.10}$$

where $\beta = \sqrt{b_{max}/b_{min}}$, the sliding condition is satisfied and implies that the system trajectories will asymptotically converge to the sliding surface from any non-zero initial state and guarantees the robust stability of the closed-loop system.

To eliminate the chattering phenomena in the conventional SMC, we use $u_{corr}(t)$ as follows and name it an improved SMC. In this algorithm, for the decreasing rate of variations of $u(t)$ around the sliding surface and in order to increase the convergence rate, the idea of using the following sliding condition is proposed (Ataei *et al.*, 2014)

$$s(\mathbf{x}(t))\dot{s}(\mathbf{x}(t)) \leqslant -\eta|s(\mathbf{x}(t))|\exp\Big(\frac{-\xi}{|s(\mathbf{x}(t))|}\Big) - \gamma s^2(\mathbf{x}(t)) \tag{2.11}$$

in which η, γ, and ξ are strictly positive constants. Using the exponential function, makes that whatever the distance of the scalar function $s(\mathbf{x}(t))$ increases from the surface, the fall rate with respect to time is greater and this action develops with an exponential factor. Also, the continuous function $\tanh(s(\mathbf{x}(t))/\varepsilon)$ is used instead of the discontinuous function $\mathrm{sgn}\,(s(\mathbf{x}(t))$ for preventing the chattering in which the parameter ε is the boundary layer thickness. By the above-mentioned description, the correction input is defined as follows for the SISO system

$$u_{corr}(t) = -\widehat{b}^{-1}(\mathbf{x}(t))w(\mathbf{x}(t)) \tag{2.12}$$

where

$$\begin{aligned} &w(\mathbf{x}(t)) = \Big[f_b + \alpha\exp\Big(-\frac{\beta}{|s(\mathbf{x}(t))|}\Big)\Big]\tanh\Big(\frac{s(\mathbf{x}(t))}{\varepsilon}\Big) + \gamma s(\mathbf{x}(t)) \\ &\alpha > \eta \qquad\qquad \alpha - \eta < 2f_b\exp\Big(-\frac{\beta}{|s(\mathbf{x}(t))|}\Big) \end{aligned} \tag{2.13}$$

Therefore, the control input is defined as

$$u(t) = \widehat{b}^{-1}(\mathbf{x}(t))[-\widehat{f}(\mathbf{x}(t)) + \ddot{x}_{desired}(t) - \lambda\dot{\tilde{x}}(t) - w(\mathbf{x}(t))] \tag{2.14}$$

2.2. MIMO system

In order to extend the method for MIMO systems, a system of second order differential equations is regarded as follows

$$\ddot{\mathbf{q}}(t) = \mathbf{f}(\mathbf{q}(t), \dot{\mathbf{q}}(t)) + \mathbf{B}(\mathbf{q}(t), \dot{\mathbf{q}}(t))\mathbf{u}(t) \tag{2.15}$$

where $\mathbf{q}(t) \in \Re^n$ is the system variable and $\mathbf{u}(t) \in \Re^n$ is the input vector and

$$\begin{aligned} &\mathbf{f}(\mathbf{q}(t), \dot{\mathbf{q}}(t)): \quad \Re^n \times \Re^n \to \Re^n \\ &\mathbf{B}(\mathbf{q}(t), \dot{\mathbf{q}}(t)): \quad \Re^n \times \Re^n \to \Re^{n\times n} \end{aligned} \tag{2.16}$$

and (2.15) is changed to the state-space form

$$\dot{\mathbf{x}}(t) = \begin{bmatrix} \dot{\mathbf{q}}(t) \\ \mathbf{f}(\mathbf{q}(t), \dot{\mathbf{q}}(t)) \end{bmatrix} + \begin{bmatrix} \mathbf{0}_{n\times n} \\ \mathbf{B}(\mathbf{q}(t), \dot{\mathbf{q}}(t)) \end{bmatrix} \mathbf{u}(t) \tag{2.17}$$

in which the state vector has the shape of $\mathbf{x}(t) = [\mathbf{q}(t), \dot{\mathbf{q}}(t)]^{\mathrm{T}}$. The maximum bound of uncertainties in system (2.2) are modified as

$$\mathbf{f}(\mathbf{x}(t)) = \widehat{\mathbf{f}}(\mathbf{x}(t)) + \overline{\boldsymbol{\Delta}}\widehat{f}(x(t)) \qquad \mathbf{B}(\mathbf{x}(t)) = (\mathbf{I} + \boldsymbol{\Delta})\widehat{\mathbf{B}}(\mathbf{x}(t)) \tag{2.18}$$

where $\overline{\boldsymbol{\Delta}}$ is the vector of the uncertainty coefficient, $\boldsymbol{\Delta}$ is a diagonal matrix of that and $\mathbf{I}$ is the identity matrix. Hence, the maximum bound of $f(\mathbf{x}(t))$ is restricted to

$$\left|\widehat{\mathbf{f}}(\mathbf{x}(t)) - \mathbf{f}(\mathbf{x}(t))\right| \leqslant \mathbf{f}_b \tag{2.19}$$

and $\mathbf{B}(\mathbf{x}(t))$ to

$$\widehat{B}_{ij}(\mathbf{x}(t)) = \sqrt{b_{max,ij} b_{min,ij}} \tag{2.20}$$

which leads to an extended form of (2.10)

$$K_i(\mathbf{x}(t)) \geqslant \beta(f_{b,i} + \eta_i) + (\beta - 1)|u_{eq,i}(t)| \tag{2.21}$$

in which $\beta = b_{max}/b_{min}$, $b_{max} = \max(b_{max,ij})$ and $b_{min} = \min(b_{\min,ij})$. $K_i(\mathbf{x}(t))$ is also the i-th diagonal element of the matrix $\mathbf{K}(\mathbf{x}(t))$. The control law of the conventional SMC possesses the shape

$$\mathbf{u}(t) = \widehat{\mathbf{B}}^{-1}(\mathbf{x}(t))[-\widehat{\mathbf{f}}(\mathbf{x}(t)) + \ddot{\mathbf{x}}_{desired}(t) - \boldsymbol{\lambda}\dot{\tilde{x}}(t)] - \widehat{\mathbf{B}}^{-1}(\mathbf{x}(t))\mathbf{K}(\mathbf{x}(t))\,\mathrm{sgn}\,(\mathbf{s}(\mathbf{x}(t)) \tag{2.22}$$

where $\mathbf{s}(\mathbf{x}(t)) = \dot{\tilde{\mathbf{x}}}(t) + \boldsymbol{\lambda}\tilde{x}(t)$. The MIMO structure of the control law of ISMC (2.14) is rewritten

$$\mathbf{u}(t) = \mathbf{B}^{-1}(\mathbf{x}(t))[-\widehat{\mathbf{f}}(\mathbf{x}(t)) + \ddot{\mathbf{x}}_{desired}(t) - \boldsymbol{\lambda}\dot{\tilde{x}}(t) - \mathbf{w}(\mathbf{x}(t))] \tag{2.23}$$

where

$$w_i(\mathbf{x}(t)) = \Big[f_{b,i} + \alpha_i \exp\Big(-\frac{\beta}{|s_i(\mathbf{x}(t))|}\Big)\Big] \tanh\Big(\frac{s_i(\mathbf{x}(t))}{\varepsilon}\Big) + \gamma_i s_i(\mathbf{x}(t)) \tag{2.24}$$

in which $\alpha_i > \eta_i$ and

$$\alpha_i - \eta_i < 2f_{b,i} \exp\Big(-\frac{\beta}{|s_i(\mathbf{x}(t))|}\Big) \tag{2.25}$$

3. Applied ISMC for the robot manipulator

Let us consider generalized coordinates of an n-link manipulator as $\mathbf{q} = \{q_1, \ldots, q_n\}$, where q_i is the generalized coordinate of the i-th joint; either revolute or prismatic. By using Lagrange's approach, the manipulator dynamical equation can be expressed as

$$\mathbf{M}_{n\times n}(\mathbf{q}(t))\ddot{\mathbf{q}}_{n\times 1}(t) + \mathbf{c}_{n\times 1}(\mathbf{q}(t), \dot{\mathbf{q}}(t)) + \mathbf{g}_{n\times 1}(\mathbf{q}(t)) = \mathbf{u}_{n\times 1}(t) \tag{3.1}$$

where $\mathbf{M}_{n\times n}(\mathbf{q}(t))$ is the inertia matrix, $\mathbf{c}_{n\times 1}(\mathbf{q}(t), \dot{\mathbf{q}}(t))$ is a vector consisting of Coriolis and centrifugal forces, $\mathbf{g}_{n\times 1}(\mathbf{q}(t))$ is the gravity force, and $\mathbf{u}_{n\times 1}(t)$ is the input vector of joints. Elements of state-space equation (2.17) are structured as

$$\begin{aligned} &\mathbf{f}(\mathbf{q}(t), \dot{\mathbf{q}}(t)) = -\mathbf{M}^{-1}(\mathbf{q}(t))[\mathbf{c}(\mathbf{q}(t), \dot{\mathbf{q}}(t)) + \mathbf{g}(\mathbf{q}(t))] \\ &\mathbf{B}(\mathbf{q}(t), \dot{\mathbf{q}}(t)) = \mathbf{M}^{-1}(\mathbf{q}(t)) \end{aligned} \tag{3.2}$$

Inserting the proposed ISMC structure into the robot equation of motion changes Eq. (2.23) into

$$\mathbf{u}(t) = \mathbf{M}(\mathbf{q}(t))\Big(\mathbf{M}^{-1}(\mathbf{q}(t))[\mathbf{c}(\mathbf{q}(t), \dot{\mathbf{q}}(t)) + \mathbf{g}(\mathbf{q}(t))] + \ddot{\mathbf{q}}_{desired}(t) - \boldsymbol{\lambda}\dot{\tilde{\mathbf{q}}}(t) - \mathbf{w}(\mathbf{s})\Big) \tag{3.3}$$

where

$$w_i(s_i) = \Big[f_{b,i} + \alpha_i \exp\Big(-\frac{\beta}{|s_i(q(t))|}\Big)\Big] \tanh\Big(\frac{s_i(q(t))}{\varepsilon}\Big) + \gamma_i s_i(q(t)) \tag{3.4}$$

in which $w_i(s_i)$ is a set as coefficients of tanh function $f_{b,i} + \alpha_i \exp[-\beta/|s_i(q(t))|]$; and $\gamma_i s_i(q(t))$ is added to the first term, $f_{b,i} + \alpha_i \exp[-\beta/|s_i(q(t))|]$ depends on the sign of $s_i(q(t))$. As shown in Fig. 1a, near the origin, $w_i(s_i)$ is equal to zero and then increases exponentially, and far from the origin converges to a constant value. Figures 1b-3b present the effect of parameters on behaviour of $w_i(s_i)$.

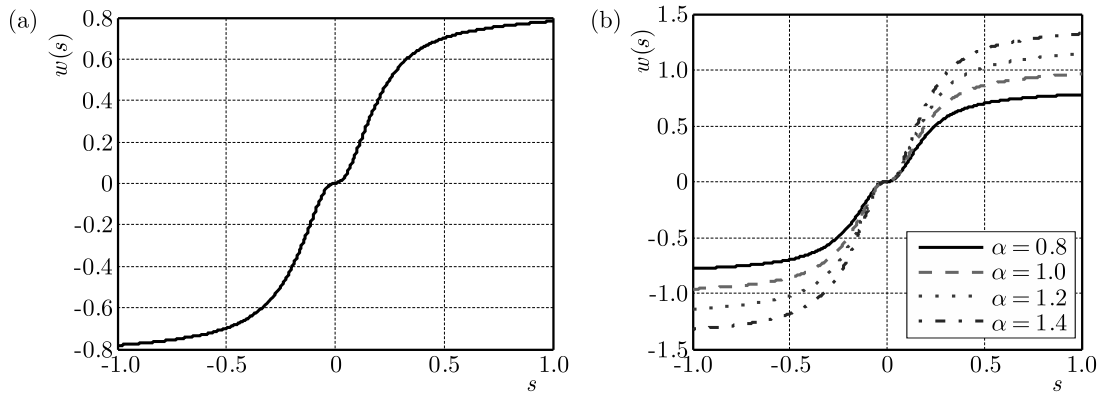

Fig. 1. (a) $w_i(s_i)$ function versus the switching function in the ISMC method; (b) changes of the design parameter α of the ISMC method in function of $w_i(s_i)$

As it is depicted in Fig. 21b, an increase in α_i results in an increase of the ultimate value of $w_i(s_i)$, but around the origin, the effect is less observable. Hence the changes of α_i do not contribute to the chartering. In Fig. 2a, an increase in β makes $w_i(s_i)$ more nonlinear near the origin and does not affect the bounds of $w_i(s_i)$, hence a steady state error might occur. The effects of changes in ε (boundary layer width) are similar to β and do not change the final value of $w_i(s_i)$, though it might lead to the steady state error, presented in Fig. 2b. Figures 3a and 3b show the similarity of f and γ behavior to α as well.

With regard to the try-and-error procedure as well as experimental and simulation study, the mentioned parameters have been designed for the 6R manipulator. The ISMC eliminates the chattering and provides more precision rather than the conventional SMC.

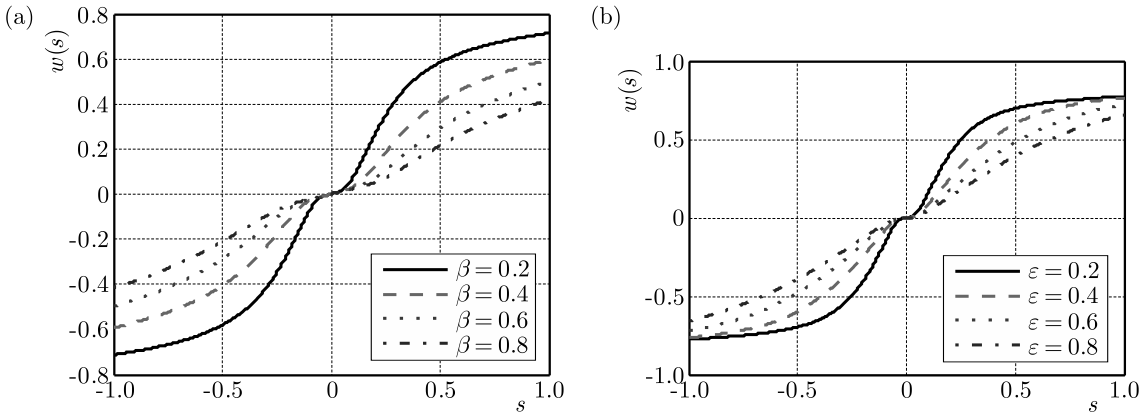

Fig. 2. Changes of the design parameter (a) β and (b) ε of the ISMC method in function of $w_i(s_i)$

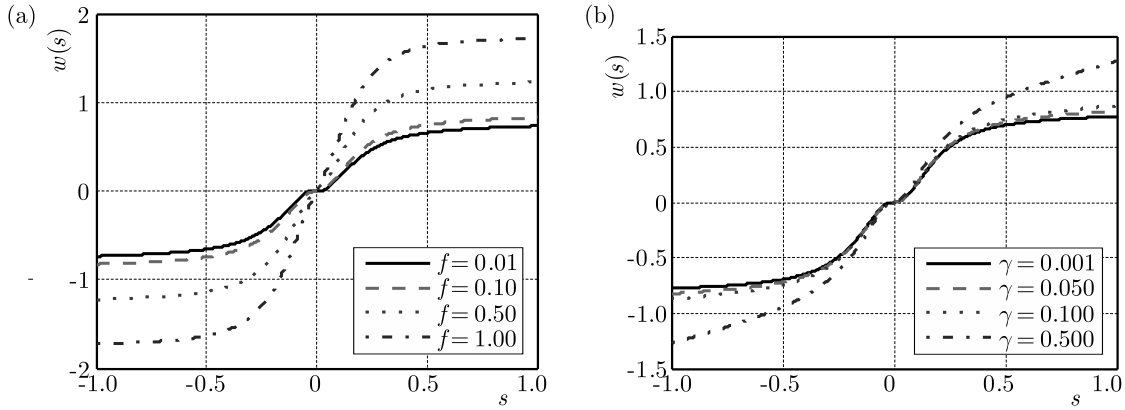

Fig. 3. Changes of the design parameter (a) f and (b) γ of the ISMC method in function of $w_i(s_i)$

4. Dynamic load carrying capacity

The dynamic load carrying capacity (DLCC) is one of the important parameters of robots that should be determined. The DLCC is described as the maximum load that a manipulator can repeatedly lift and carry on the extended configuration in a particular path with an acceptable tracking accuracy. The DLCC is a useful criterion for the assessment of different controllers on the same arm, especially for the estimation of energy consumption and efficiency. The DLCC of a manipulator calculates with respect to the limitation of motors and error of the final point in a finite time. Upper and lower limits of motor torques can be computed from

$$u_{max,i}(t) = u_{s,i} - \frac{u_{s,i}}{\omega_{nl,i}}\dot{q}_i(t) \qquad u_{min,i}(t) = -u_{s,i} - \frac{u_{s,i}}{\omega_{nl,i}}\dot{q}_i(t) \tag{4.1}$$

where $u_{s,i}$ is the stall torque of the i-th motor, $\omega_{nl,i}$ is no-load speed of that and $\dot{q}_i(t)$ is actual rotational speed of the motor. In the point-to-point motion, the carrying load increases until the error of the final point in a finite time reaches the allowable bound, while in trajectory tracking, it increases until the torques of motors touch the bounds of limitations. The algorithm of finding the DLCC is shown in Fig. 4.

5. Model of 6R manipulator

5.1. Mechanical structure

The case study of this article is a 6R manipulator with six revolute joints that have massive and complex dynamic and uncertainty in the modelling that shows the capability of the purposed

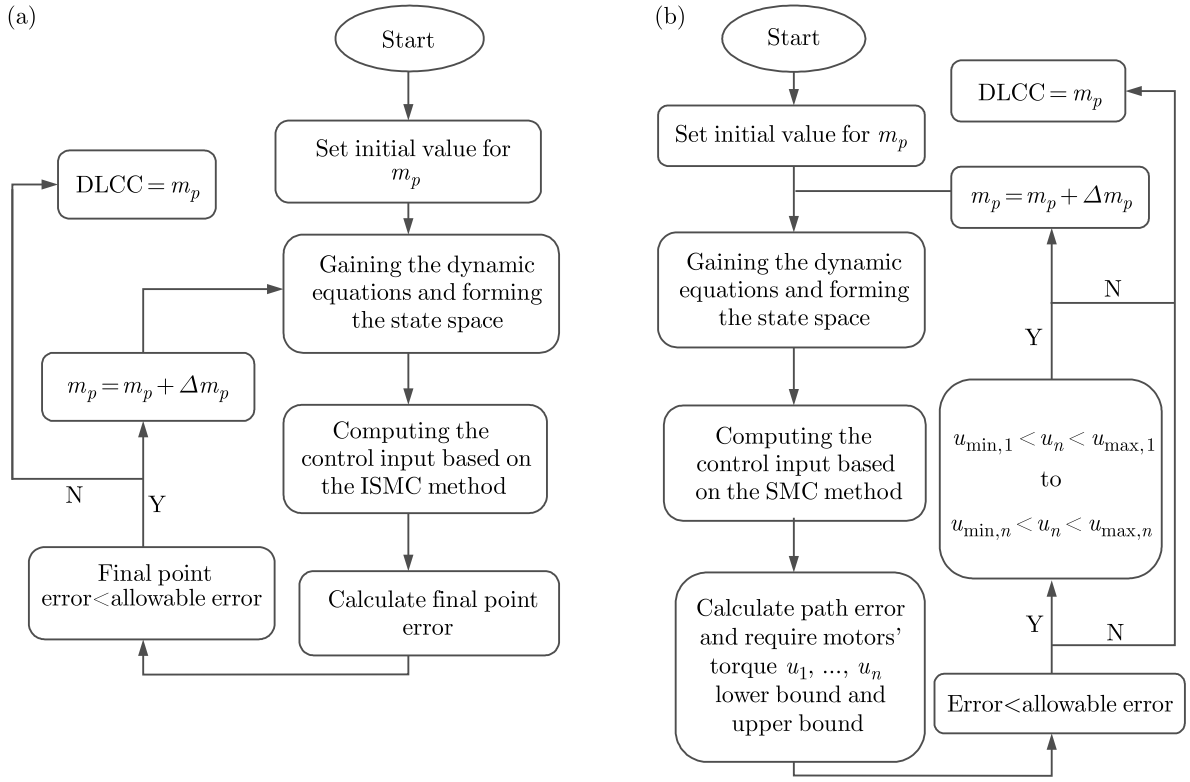

Fig. 4. Algorithms for finding DLCC: (a) point-to-point motion and (b) trajectory tracking

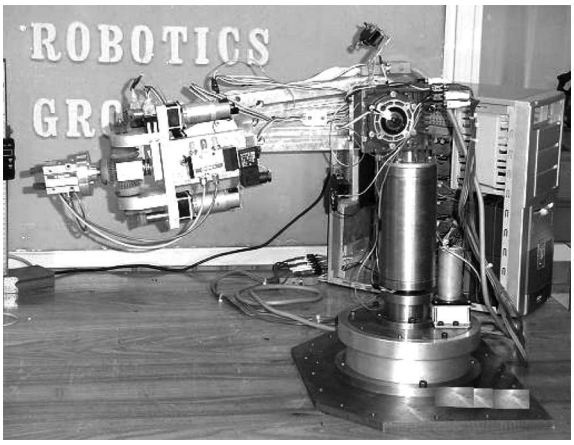

Fig. 5. 6R manipulator (Korayem *et al.*, 2013)

controller. Figure 5 presents the 6R manipulator. Figure 6 shows a schematic of the robot. The Denavit-Hartenberg parameters of the robot are presented in Table 1.

Korayem *et al.* (2013) described the forward kinematics, inverse kinematics, and Jacobian matrix of 6R. The hardware of the previous controller (Korayem *et al.*, 2010) was improved to perform the nonlinear methods better. The new developed digital board of 6R (Korayem *et al.*, 2013) consists of LPC1768 ARM microcontroller. This board is capable of computing massive programs with adequate speed. In the next Subsection, the structure of hardware is explained to a greater extent.

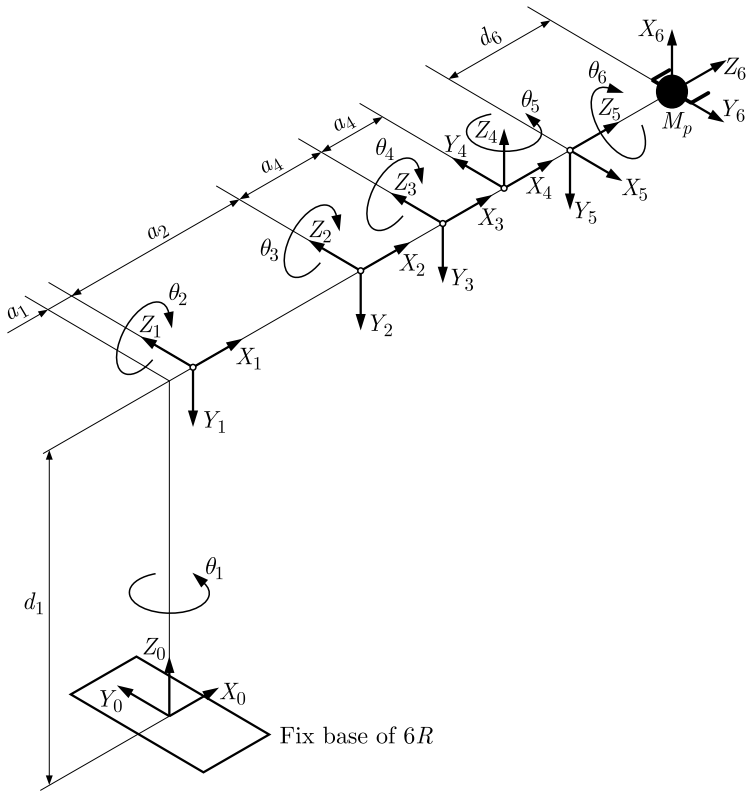

Fig. 6. Schematic of 6R manipulator (Korayem *et al.*, 2013)

Table 1. The Denavit-Hartenberg parameters of 6R arm

Joint i	a_i [mm]	d_i [mm]	α_i [°]
1	0	438	−90
2	251.5	0	0
3	125	0	0
4	92	0	90
5	0	0	−90
6	0	152.8	0

5.2. Hardware of controller

The old system of the controller of 6R was built in a way to perform open loop control (Ahmadi *et al.*, 2009), and it needed an alternative electronic controller unit (ECU) to upgrade the whole system to a closed loop level. The previous ECU was based on PIC microcontrollers; the system used six PIC chips to perform the task. The new 6R robot main board consists of LPC1768 microcontroller, input feedback read, PWM output, and digital communications. LPC1768 is a 32 bit microcontroller based on ARM Cortex M3 processor which operates at up to 100 MHz frequency. This microcontroller has 100 pins, which are allowed to manage driving of six motors easily, and a 12-bit A/D to give feedback on the position of links to the processor. The processor has also six pins for generating different PWMs that enable motors to drive in both directions (Korayem *et al.*, 2013).

The main board duty is to compute and apply the algorithms and for driving the motors, but another board needs to be used. The driver board of motors is an other section of the setup. BTS7810 having H-bridge design is chosen for driving the motors. This driver is capable of providing 40 A and 48 V. Six potentiometers as the feedback are placed on the joints. The

sensitivity and speed of the response are two important items in this part. The voltage of each potentiometer separately passes through a low pass filter and after that an ADC channel converts the voltage to data. The commands are initiated in computers and then are sent to LPC1768. Next, the error is computed by comparing the position of current angles and desired ones. Derivative of the error is computed approximately by division of two consecutive data on the sample time. Then, the control signals are sent to motor drivers to provide the needed power for DC motors.

6. Simulation and experimental result

6.1. Illustrative example

For the assurance of preference of the ISMC method, in this part of article, we compare this method with the conventional SMC and use it for the two-link manipulator as an illustrative example. The schematic of the two-link manipulator is shown in Fig. 7. The parameters of the two-link manipulator are illustrated in Table 2, and the parameters of conventional SMC are considered as $K_1 = K_2 = 10$ and $\lambda_1 = \lambda_2 = 2$; and ISMC coefficients are considered as $f_{b,1} = f_{b,2} = 250$, $\alpha_1 = \alpha_2 = 50$, and $\beta = 500$, $\gamma_1 = \gamma_2 = 10$, $\varepsilon = 0.5$ and $\lambda_1 = \lambda_2 = 2$. Figure 8 shows the end-effector tracking. Figure 9 shows the path error of two methods, and Figs. 10a and 10b show the correction input of the first and second joint of the two methods that caused chattering.

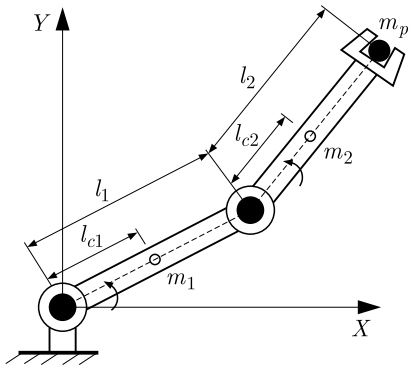

Fig. 7. Schematic of the two-link manipulator

Table 2. Parameters of the two link manipulator

l_1	l_2	l_{c1}	l_{c2}	m_1	m_2	m_p	I_1	I_2
1 m	1 m	0.5 m	0.5 m	2 kg	2 kg	0.5 kg	0.166 kgm^2	0.166 kgm^2

As it is shown in the results, by considering $m_p = 0.1$ kg as the external disturbance, the main distinction between conventional and improved SMC could be directed in chattering reduction topic, which eventually leads to more precision, while less energy is consumed by the actuators.

The point is evident in Figs. 9 and 10; however, to have a clearer view in the matter, Table 3 is arranged for more information in terms of norms of inputs and errors of the system.

6.2. 6R manipulator

In this Section, the results of simulation and experimental tests on the 6R manipulator are presented. For simulation, the dynamical equation of the robot is generated as differential equations and solved with MATLAB software. The motor characteristics are given in Table 4.

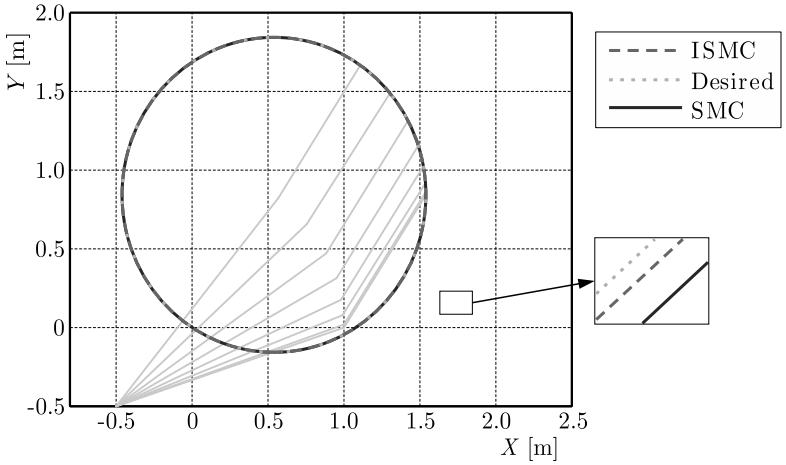

Fig. 8. Trajectories and configuration of the two-link arm

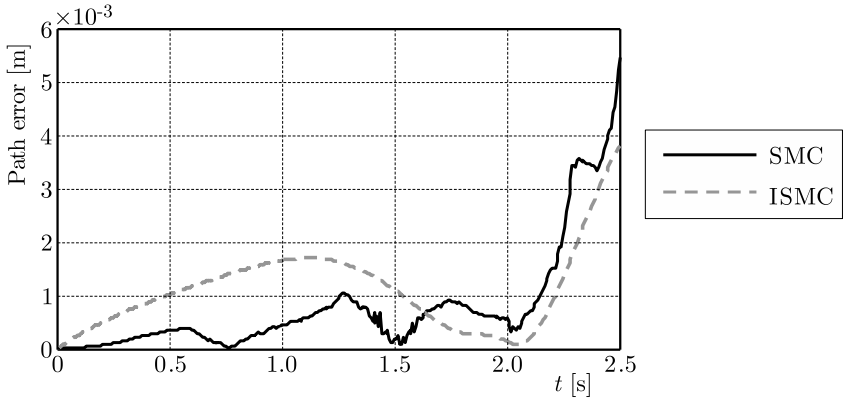

Fig. 9. Error of path tracking of the planar robot

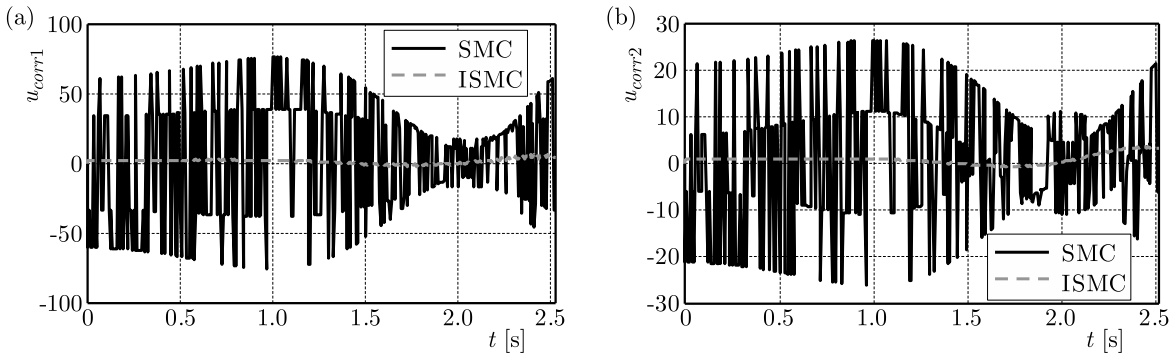

Fig. 10. Correction input of the (a) first link and (b) second link, two-link arm

Table 3. Comparison of errors in inputs and end-effectors between ISMC and SMC of the planar robot

Methods	Max $\|u_1\|$ [N·m]	Max $\|u_2\|$ [N·m]	Maximum error [m]
SMC	127.1296	51.5406	0.0054
ISMC	6.8886	3.3870	0.0023

Table 4. Specifications of motors of the 6R robot

Motor	1	2	3	4	5	6
u_s [N·m]	114	98	382.2	40.4	40.4	40.4
ω_{nl} [rad/s]	1.3	1.04	0.73	0.9	0.9	0.9

The torque equation is calculated in a parametric form and programmed in the microcontroller to change to the PWM voltage level. The computed voltages are sent to the motors in real time, and the measured feedback of potentiometers is sent to the main board. This process continues till the error sets in the allowable bound. Then, the values which are obtained from the potentiometers are stored in the main PC.

6.2.1. Point-to-point motion

Point-to-point motion starts from point $A(0.0533, 0.4585, 0.4033)$ and ends with point $B(0.5264, 0.07115, 0.5885)$ during 6 s. The parameters of the SMC controller are given in Table 5 by experiments. Figure 11 shows the end-effector trajectories theoretically and experimentally. In Fig. 12, the variation angles of links are shown. The comparison of simulation results with experiments show sufficient accuracy. The difference between the actual angles and desired ones is due to clearances in the gearbox. Figure 13 shows the chattering reduction and smoothness of ISMC as the main controller for the experimental implementation with respect to the conventional SMC in point-to-point motion.

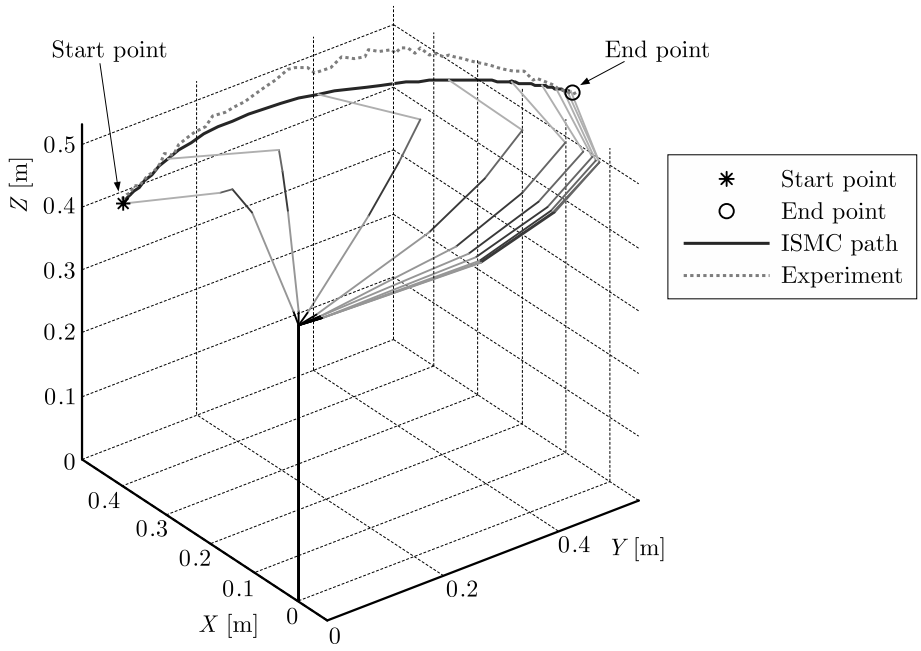

Fig. 11. ISMC point-to-point motion of the 6R robot via simulation and experiment

Regarding the solid structure and heavy links of the 6R manipulator, the conventional SMC has only been implemented theoretically. In experiments, the ISMC method has been applied in the 6R robot to reduce the risk of any defect to motors brought up by probable chattering of SMC. For the error of the end point in a finite time, the allowable bound is given as $\delta = 0.02$. By this constraint, DLCC is obtained to be about 920 g.

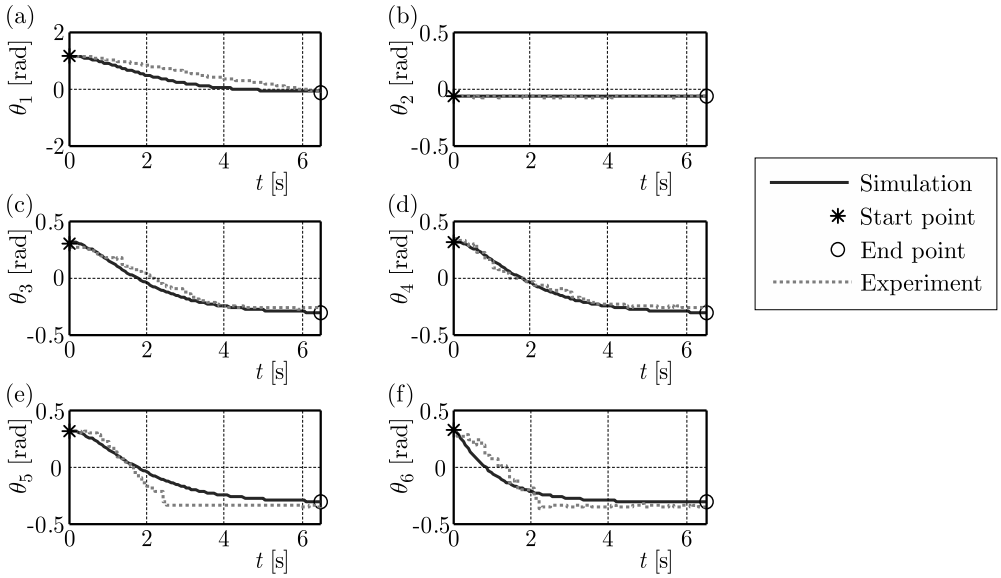

Fig. 12. Angle of links in ISMC point-to-point motion of the 6R robot

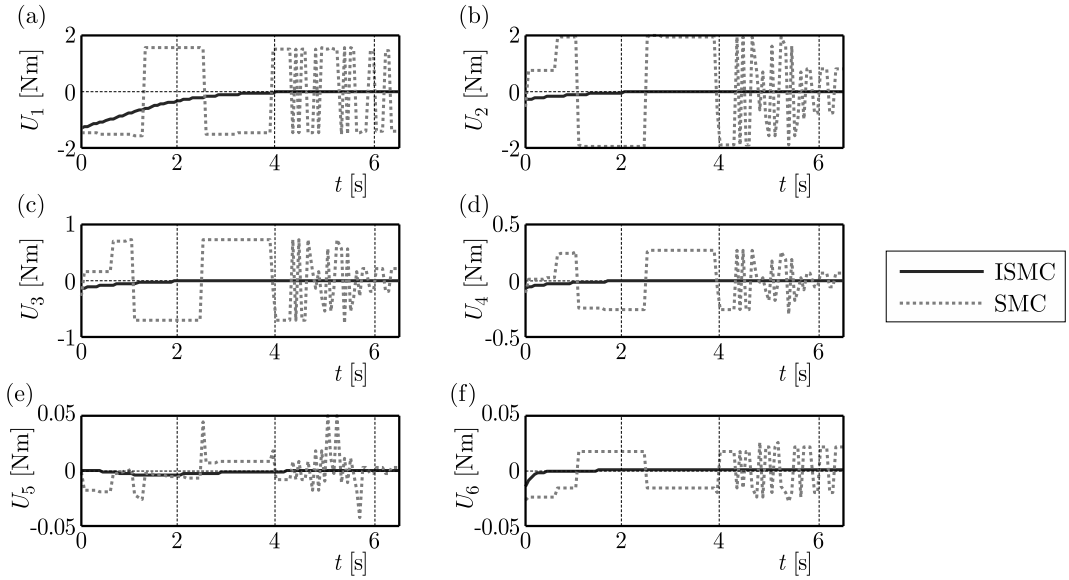

Fig. 13. Theoretical comparison of SMC and ISMC for actuators of the 6R robot

Table 5. Parameters of the ISMC controller for point-to-point motion of the 6R robot

Joint number	λ	f_b	α	β	γ	ε
1	10	10	2	10	0.01	0.5
2	10	10	2	10	0.01	0.5
3	10	10	2	10	0.01	0.5
4	10	10	2	10	0.01	0.5
5	10	50	2	10	0.01	0.5
6	10	50	2	10	0.01	0.5

6.2.2. Trajectory tracking

The trajectory tracking has also been performed in a circular path. Equations of the desired path are given as follows

$$x_e(t) = \frac{7}{9315}t^5 - \frac{1}{1242}t^4 - \frac{5}{621}t^3 + \frac{5}{10} \qquad y_e(t) = -\frac{14}{9315}t^5 + \frac{1}{621}t^4 + \frac{10}{621}t^3 + \frac{1}{10}$$
$$z_e(t) = -\frac{7}{9315}t^5 + \frac{1}{1242}t^4 + \frac{5}{621}t^3 + \frac{6}{10}$$

The initial conditions are defined as

$$x(0) = \begin{bmatrix} -0.1 & -0.44 & 0.2 & 0.65 & -1.1 & 0 & \mathbf{0}_{1\times 6} \end{bmatrix}^{\mathrm{T}}$$

The best parameters for the SMC controller in this path are given in Table 6 through experiments. Figure 14 shows the end-effector trajectory both theoretically and experimentally. In Fig. 15, the variations of angles of links are shown, and in Fig. 6, angular velocities are shown.

Table 6. Parameters of the ISMC controller for trajectory tracking of the 6R robot

Joint number	λ	f_b	α	β	γ	ε
1	10	100	2	10	0.01	0.5
2	10	100	2	10	0.01	0.5
3	10	100	2	10	0.01	0.5
4	10	100	2	10	0.01	0.5
5	10	150	2	10	0.01	0.5
6	10	150	2	10	0.01	0.5

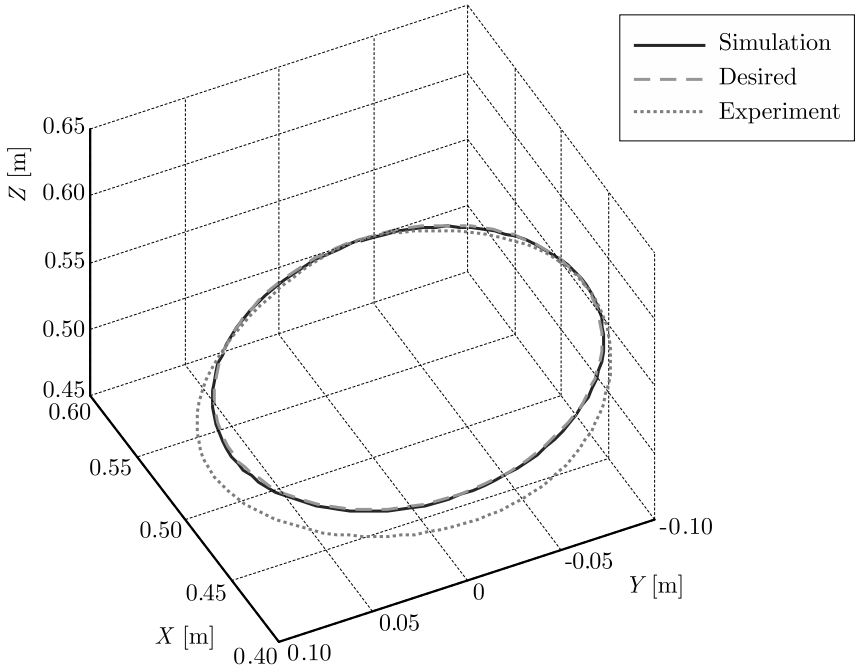

Fig. 14. ISMC trajectory tracking of the 6R robot via simulation and experiment

In the trajectory tracking, DLCC is calculated with respect to the limitation of motors and error path. In Fig. 17, the control inputs are shown. The allowable error is considered 10 mm. As it is shown, the torque of the third motor reaches its lower bound. The DLCC in this trajectory is obtained to be 700 g.

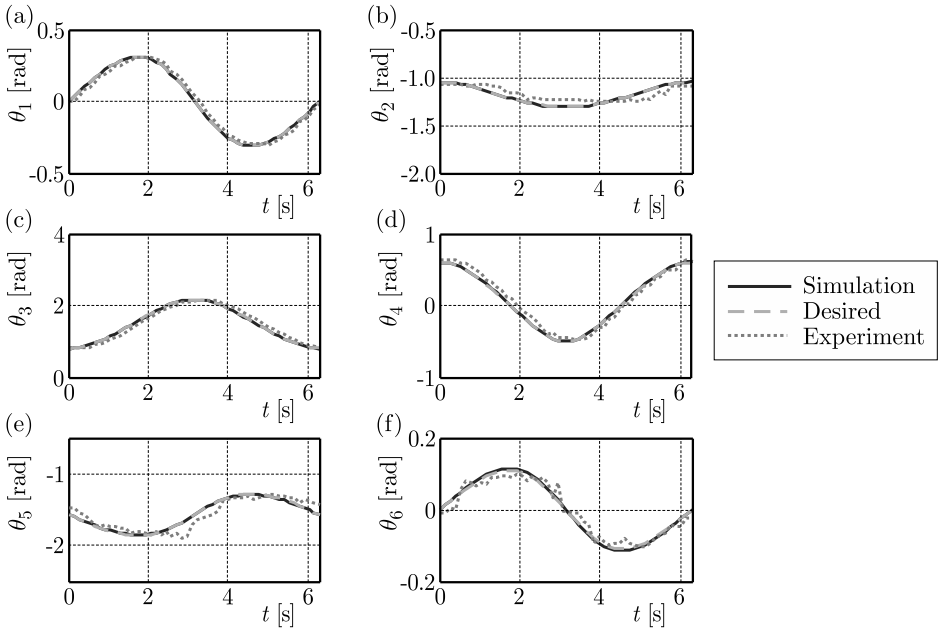

Fig. 15. Angle of links in ISMC trajectory tracking of the 6R robot

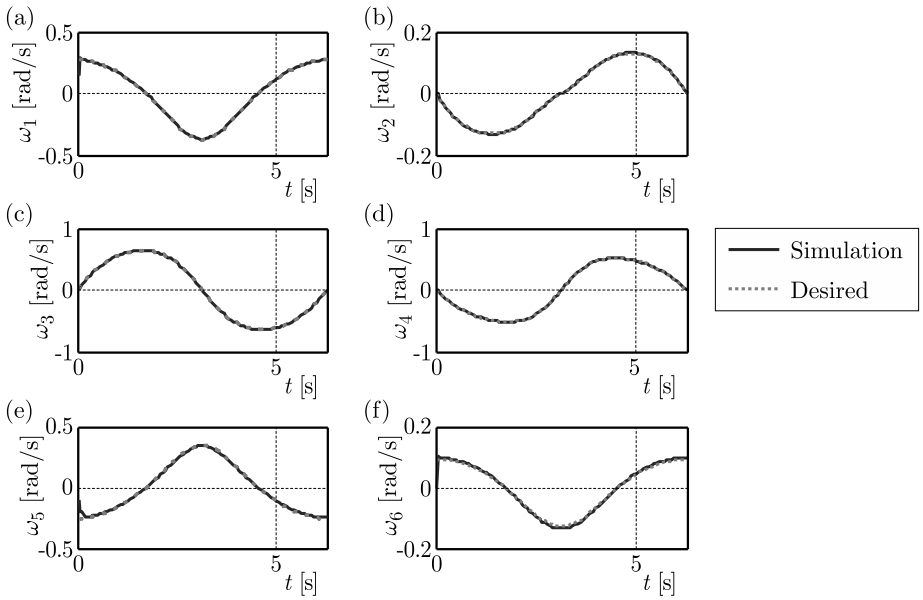

Fig. 16. Angular velocities of links in ISMC trajectory tracking of the 6R robot

7. Conclusions

In this work, we have designed the improved sliding mode control method for manipulators and studied the effect of various parameters on the behaviour of the ISMC controller. First, the ISMC method was simulated for the two-link manipulator for the assurance of good performance and then was implemented to the 6R manipulator as a good case study. The new hardware of robot based on LPC1768 ARM microcontroller allowed performing massive calculation of dynamics and closed loop control of the 6R manipulator. The point-to-point motion and trajectory tracking problems were compared with experimental results. A good performance for manipulator control in the presence of modelling the uncertainty and disturbance was confirmed. The main problem of SMC was the chattering phenomenon, and as a result, the IMSC method provided smooth

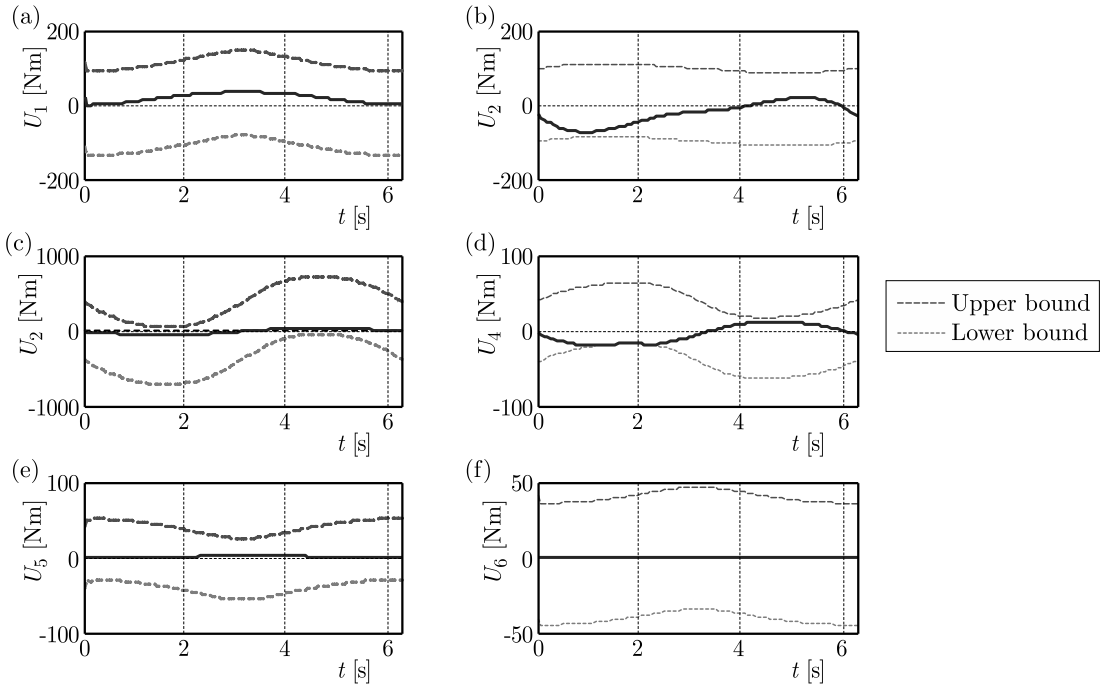

Fig. 17. Control inputs of ISMC trajectory tracking of the 6R robot

input torques for robot motors. Also, the dynamic load carrying capacity for the 6R robot in point-to-point motion and trajectory tracking was increased by considering the robustness of the controller.

References

1. Ahmadi R., Korayem M.H., Jaafari N., Jamali Y., Kiomarsi M., Habibnejad A., 2009, Design, modeling, implementation and experimental analysis of 6R robot, *International Journal of Engineering Science*, **21**, 1, 71-84

2. Ataei M., Hooshmand R.A., Samani S.G., 2014, A coordinated MIMO control design for a power plant using improved sliding mode controller, *ISA Transactions*, **53**, 2, 415-422

3. Beyhan S., Lendek Z., Babuska R., Wisse M., Alci M., 2011, Adaptive fuzzy and sliding--mode control of a robot manipulator with varying payload, *Proceeding of IEEE Conference on Decision and Control and European Control Conference*, Orlando, FL, USA, 8291-8296

4. Capisani L.M., Ferrara A., 2012, Trajectory planning and second-order sliding mode motion/interaction control for robot manipulators in unknown environments, *IEEE Transactions on Industrial Electronics*, **59**, 8, 3189-3198

5. Ertugrul M., Kaynak O., Keresteciogl u F., 2000, Gain adaptation in sliding mode control of robotic manipulators, *International Journal of Systems Science*, **31**, 9, 1099-1106

6. Foster D., Harrison A., 2011, Experimental investigation of a 5-DOF robot arm with sliding mode control, *Proceeding of IEEE Conference on Robotics, Automation and Mechatronics*, Qingdao, 125-130

7. Hamraz N.J., Korayem M.H., Jamali Y., Kiumarsi M., Asadi M.A., Rezaei S., Sohrabi A., 2005, Design, manufacturing and performance testing of 3r manipulator, *International Congress on Manufacturing Engineering*, Tehran

8. Islam S., Liu X.P., 2011, Robust sliding mode control for robot manipulators, *IEEE Transactions on Industrial Electronics*, **58**, 6, 2444-2453

9. Islam R.U., Iqbal J., Khan Q., 2014, Design and comparison of two control strategies for multi--DOF articulated robotic arm manipulator, *Journal of Control Engineering and Applied Informatics*, **16**, 2, 28-39

10. Jamali Y., Korayem M.H., Hamraz N.J., Sohrabi A.M., Kiomarsi M., Asadi M.A., Reazaee S., 2005, Design and manufacturing a robot wrist: performance analysis, *International Congress on Manufacturing Engineering*, Tehran

11. Korayem M.H., Haghighi R., Nikoobin A., Alamdari A., Korayem A.H., 2009, Determining maximum load carrying capacity of flexible link manipulators, *Scientia Iranica, Transactions B: Mechanical Engineering*, **16**, 5, 440-450

12. Korayem M.H., Irani M., Nekoo S.R., 2010, Analysis of manipulators using SDRE: A closed loop nonlinear optimal control approach, *Scientia Iranica, Transaction B: Mechanical Engineering*, **17**, 6, 456-467

13. Korayem M.H., Nekoo S.R., Abdollahi F., 2013, Hardware implementation of a closed loop controller on 6R robot using ARM microcontroller, *International Research Journal of Applied and Basic Sciences*, **4**, 8, 2147-2158

14. Korayem M.H., Khademi A., Nekoo S.R., 2014, A comparative study on SMC, OSMC and SDRE for robot control, *IEEE Second RSI/ISM International Conference on Robotics and Mechatronics (ICRoM)*, Tehran, Iran, 013-018

15. Sefriti S., Boumhidi J., Naoual R., Boumhidi I., 2012, Adaptive neural network sliding mode control for electrically-driven robot manipulators, *Journal of Control Engineering and Applied Informatics*, **14**, 4, 27-32

16. Shi J., Liu H., Bajcinca N., 2008, Robust control of robotic manipulators based on integral sliding mode, *International Journal of Control*, **81**, 10, 1537-1548

17. Slotine J.J.E., Li W., 1991, *Applied Nonlinear Control*, Vol. 60, Englewood Cliffs, NJ: Prentice--Hall

18. Thangavelusamy D., Ponnusamy L., 2013, Elimination of chattering using fuzzy sliding mode controller for drum boiler turbine System, *Journal of Control Engineering and Applied Informatics*, **15**, 2, 78-85

19. Vega V.P., Arimoto S., Liu Y.H., Hirzinger G., Akella P., 2003, Dynamic sliding PID control for tracking of robot manipulators: theory and experiments, *IEEE Transactions on Robotics and Automation*, **19**, 6, 967-976

Manuscript received August 24, 2015; accepted for print August 12, 2016